jove

Measurement of the Directional Information Flow in fNIRS-Hyperscanning Data using the Partial Wavelet Transform Coherence Method

Siyuan Zhou[*,1], **Yuhang Long**[*,2], **Chunming Lu**[1]

[1] State Key Laboratory of Cognitive Neuroscience and Learning & IDG/McGovern Institute for Brain Research, Beijing Normal University [2] Institute of Developmental Psychology, Faculty of Psychology, Beijing Normal University

[*] These authors contributed equally

Corresponding Author

Chunming Lu
luchunming@bnu.edu.cn

Citation

Zhou, S., Long, Y., Lu, C. Measurement of the Directional Information Flow in fNIRS-Hyperscanning Data using the Partial Wavelet Transform Coherence Method. *J. Vis. Exp.* (175), e62927, doi:10.3791/62927 (2021).

Date Published

September 3, 2021

DOI

10.3791/62927

URL

jove.com/video/62927

Abstract

Social interaction is of vital importance for human beings. While the hyperscanning approach has been extensively used to study interpersonal neural synchronization (INS) during social interactions, functional near-infrared spectroscopy (fNIRS) is one of the most popular techniques for hyperscanning naturalistic social interactions because of its relatively high spatial resolution, sound anatomical localization, and exceptionally high tolerance of motion artifacts. Previous fNIRS-based hyperscanning studies usually calculate a time-lagged INS using wavelet transform coherence (WTC) to describe the direction and temporal pattern of information flow between individuals. However, the results of this method might be confounded by the autocorrelation effect of the fNIRS signal of each individual. For addressing this issue, a method termed partial wavelet transform coherence (pWTC) was introduced, which aimed to remove the autocorrelation effect and maintain the high temporal-spectrum resolution of the fNIRS signal. In this study, a simulation experiment was performed first to show the effectiveness of the pWTC in removing the impact of autocorrelation on INS. Then, step-by-step guidance was offered on the operation of the pWTC based on the fNIRS dataset from a social interaction experiment. Additionally, a comparison between the pWTC method and the traditional WTC method and that between the pWTC method and the Granger causality (GC) method was drawn. The results showed that pWTC could be used to determine the INS difference between different experimental conditions and INS's directional and temporal pattern between individuals during naturalistic social interactions. Moreover, it provides better temporal and frequency resolution than the traditional WTC and better flexibility than the GC

method. Thus, pWTC is a strong candidate for inferring the direction and temporal pattern of information flow between individuals during naturalistic social interactions.

Introduction

Social interaction is of vital importance for human beings[1,2]. For understanding the dual-brain neurocognitive mechanism of social interaction, the hyperscanning approach has recently been extensively used, showing that the patterns of interpersonal neural synchronization (INS) can well characterize the social interaction process[3,4,5,6,7,8,9,10,11,12,13,14]. Among recent studies, an interesting finding is that the role difference of individuals in a dyad may lead to a time-lagged pattern of INS, i.e., INS occurs when the brain activity of one individual lags behind that of another individual by seconds, such as that from listeners to speakers[5,9], from leaders to followers[4], from teachers to students[8], from mothers to children[13,15], and from women to men in a romantic couple[6]. Most importantly, there is a good correspondence between the interval of the time-lagged INS and that of social interaction behaviors, such as between teachers questioning and students answering[8] or between parenting behaviors of mothers and compliance behaviors of children[15]. Thus, time-lagged INS may reflect a directional information flow from one individual to another, as proposed in a recent hierarchical model for interpersonal verbal communication[16].

Previously, the time-lagged INS was mainly calculated on the functional near-infrared spectroscopy (fNIRS) signal because of its relatively high spatial resolution, sound anatomical localization, and exceptionally high tolerance of motion artifacts[17] when studying naturalistic social interactions. Moreover, to precisely characterize the correspondence between the neural time lag and the behavioral time lag during social interaction, it is essential to obtain the INS strength for each time lag (e.g., from no time lag to a time lag of 10 s). For this purpose, previously, the wavelet transform coherence (WTC) procedure was extensively applied after shifting the brain signal of one individual forward or backward relative to that of another individual[5,6,18]. When using this traditional WTC procedure for fNIRS signals, there is a potential challenge because the observed time-lagged INS may be confounded by the autocorrelation effect of the fNIRS signal for an individual[19,20,21]. For example, during a dyadic social interaction process, the signal of participant A at time point *t* may be synchronized with that of participant B at the same time point. Meanwhile, the signal of participant A at time point *t* may be synchronized with that of participant A at a later time point *t*+1 because of the autocorrelation effect. Therefore, a spurious time-lagged INS may occur between the signal of participant A at time point *t* and that of participant B at time point *t*+1.

Mihanović and his colleagues[22] first introduced a method termed partial wavelet transform coherence (pWTC), and then applied it in marine science[23,24]. The original purpose of this method was to control the exogenous confounding noise when estimating the coherence of two signals. Here, to address the autocorrelation issue in the fNIRS hyperscanning data, the pWTC method was extended to calculate time-lagged INS on the fNIRS signal. Precisely, a time-lagged INS (and a directional information flow) from participant A to participant B can be calculated using the equation below (**Equation 1**)[23].

$$pWTC_{BtoA} = \frac{\left|\sqrt{WTC(B_t,A_{t+n})} - \sqrt{WTC(A_t,A_{t+n})} \cdot \sqrt{WTC(A_t,B_t)}^{*}\right|^2}{[1\text{-}WTC(A_t,A_{t+n})] \cdot [1\text{-}WTC(A_t,B_t)]}$$

Here, it is assumed that there are two signals, *A* and *B,* from participants A and B, respectively. The occurrence of signal *B* always precedes that of signal *A* with a time lag of *n*, where *WTC* (A_t, B_{t+n}) is the traditional time-lagged WTC. *WTC* (A_t, A_{t+n}) is the autocorrelated WTC in participant A. *WTC* (A_t, B_t) is the time-aligned WTC at time point *t* between participant A and B. * is the complex conjugate operator (**Figure 1A**).

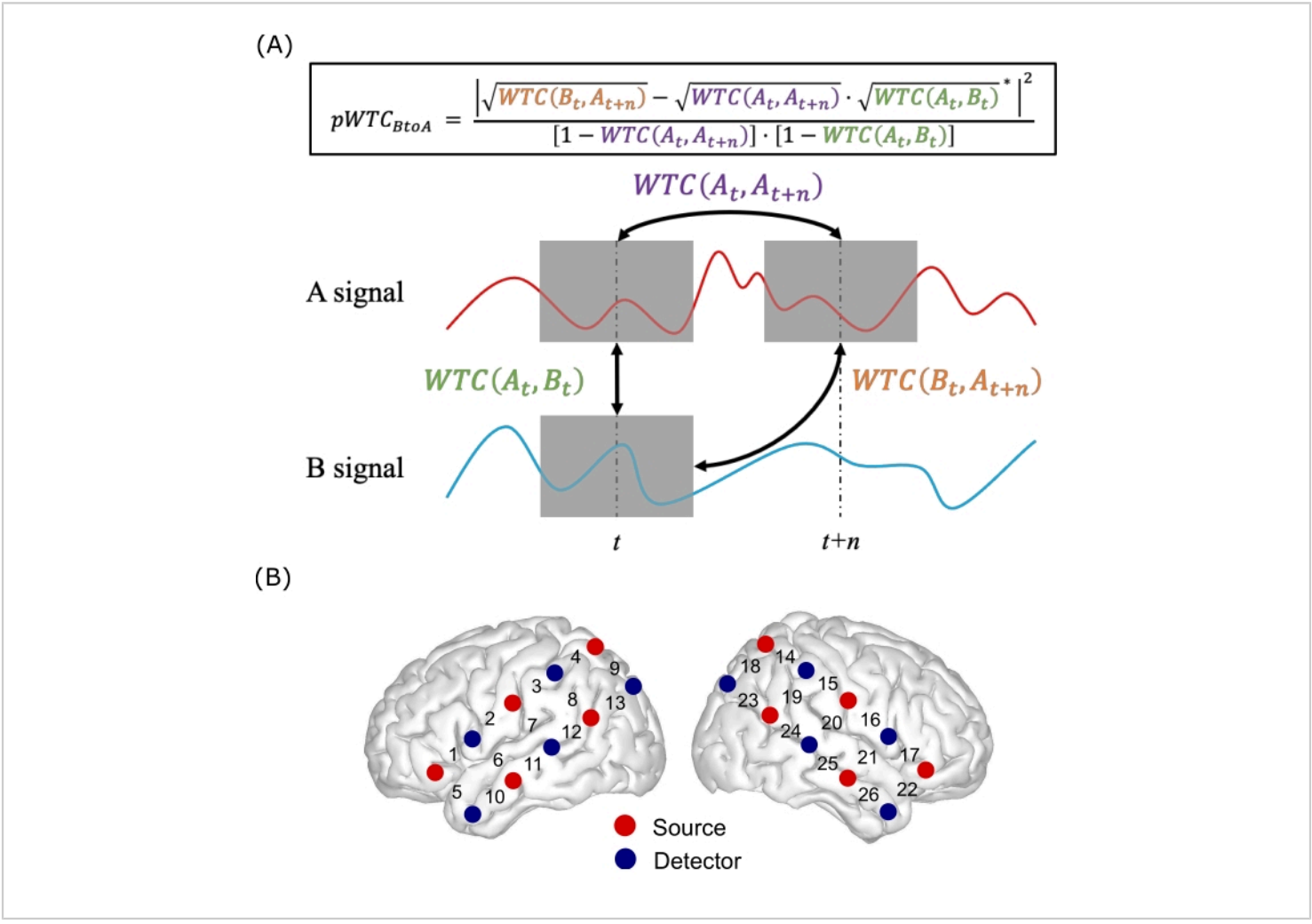

Figure 1: Overview of pWTC. (**A**) The logic of the pWTC. There are two signals *A* and *B,* within a dyad. The occurrence of *A* always follows that of *B* with a lag *n*. A gray box is a wavelet window at a certain time point *t* or *t+n*. Based on the pWTC equation (represented in the figure), three WTCs need to be calculated: the time-lagged WTC of A_{t+n} and B_t; the autocorrelated WTC in participant A of A_t and A_{t+n}; and the time-aligned WTC at timepoint *t*, A_t and B_t. (**B**)The layout of optode probe sets. CH11 was placed at T3, and CH25 was placed at T4 following the international 10-20 system[27,28].

Please click here to view a larger version of this figure.

This protocol first introduced a simulation experiment to demonstrate how well the pWTC resolves the autocorrelation challenge. Then, it explained how to conduct pWTC in a step-by-step way based on an empirical experiment of naturalistic social interactions. Here, a communication context was used to introduce the method. This is because, previously, the time-lagged INS was usually calculated in a naturalistic communication context[3,4,6,8,13,15,18]. Additionally, a comparison between the pWTC and the traditional WTC and validation with the Granger causality (GC) test were also conducted.

Protocol

The human experiment protocol was approved by the Institutional Review Board and Ethics Committee of the State Key Laboratory of Cognitive Neuroscience and Learning at Beijing Normal University. All participants gave written informed consent before the experiment began.

1. The simulation experiment

1. Generate two time series of signals that correlate with each other, with one signal having autocorrelation at a 4 s time lag. Set the correlation coefficient of r between the two signals to 0.4.
2. Furthermore, generate two time series of signals without any correlation but with autocorrelation in one signal.
3. Calculate values of traditional 4 s time-lagged INS with **Equation 2** based on the generated signals with or without correlation, which can be named time-lagged INS_{WTC} with autocorrelation and time-lagged baseline INS_{WTC} with autocorrelation.

   NOTE: Here, the traditional time-lagged WTC is expressed by the following equation (**Equation 2**)[25]

$$WTC(W_t,M_{t+n}) = \frac{|S(C^*_{W_t}(i,t)\cdot C_{M_{t+n}}(i,t))|^2}{S(|C_{W_t}(i,t)|^2)\cdot S(|C_{M_{t+n}}(i,t)|^2)}$$

   where, *C* denotes the continuous wavelet transform operator at different scales *i* and time points *t*. *S* denotes the smoothing operator. * denotes the complex conjugate operator. W and M indicate two individual time series of signals.
4. Remove autocorrelation from the generated signals. Then, calculate the values of traditional 4 s time-lagged INS_{WTC} with **Equation 2** based on the generated signals with or without correlation, which can be named time-lagged INS_{WTC} without autocorrelation and time-lagged baseline INSWTC without autocorrelation.
5. Calculate the values of 4 s time-lagged pWTC with **Equation 3** based on the generated signals with or without correlation, named time-lagged INS_{pWTC} and time-lagged baseline INS_{pWTC}.

   NOTE: The pWTC can be calculated based on the following equation (**Equation 3**)[23]

$$pWTC_{WtoM} = \frac{\left|\sqrt{WTC(W_t,M_{t+n})}\cdot\sqrt{WTC(M_t,M_{t+n})}\cdot\sqrt{WTC(W_t,M_t)}^*\right|^2}{[1-WTC(M_t,M_{t+n})]\cdot[1-WTC(W_t,M_t)]}$$

   where, *WTC* (W_t, M_{t+n}) is the traditional time-lagged WTC. *WTC* (M_t, M_{t+n}) is the autocorrelated WTC of one individual. *WTC* (W_t, M_t) is the time-aligned WTC. * is the complex conjugate operator.
6. Repeat the above procedures 1000 times.
7. After subtracting the baseline INS, compare the results of time-lagged INS_{WTC} with autocorrelation, time-lagged INSWTC without autocorrelation, and time-lagged INS_{pWTC} using the analyses of variance (ANOVA) method.

NOTE: Here, it is expected that the time-lagged INS_{WTC} with autocorrelation will be significantly higher than the time-lagged INS_{WTC} without autocorrelation and the time-lagged INS_{pWTC}, and no significant difference is expected between the time-lagged INS_{WTC} without autocorrelation and the time-lagged INS_{pWTC}.

2. The empirical experiment

1. Participants and procedure
    1. Recruit appropriate participants.
        NOTE: In this study, twenty-two pairs of close opposite-sex friends (mean age of women = 20.95, standard deviation (SD) = 1.86; mean age of men = 20.50, SD = 1.74) were recruited through advertising from undergraduates of universities in Beijing. All participants were right-handed and had normal or corrected-to-normal vision. Furthermore, no participants had any language, neurological, or psychiatric disorders.
    2. Ask each pair of participants to sit face-to-face during the experiment. Ask them to communicate freely on a supportive topic in one session and on a conflict topic in the other session.
        NOTE: The topics were used to induce the intended positive or negative emotional valence. Each communication session lasted 10 min, and the order of topics was counterbalanced.
    3. Ask the participants to report about the supportive and the conflict topics as a standard set-up rule. Ask each partner to rate the positive or negative valence level that might have been induced on a definite point scale. Then, rank the reported topics according to the rating.
        NOTE: In this work, the topics were selected with the following three steps. First, for the supportive topics, each participant was required to report 1-3 personal issues related to what she/he wanted to improve in her/his life. Each participant was required to report 1-3 cases that had induced or would induce conflict between them or that might endanger their relationship for the conflict topics. Second, each partner was required to rate the level of positive or negative valence each topic might induce on a 7-point scale (1 = not at all, and 7 = very much). Third, the reported topics were ranked according to the rating. The first two topics in the list of supportive topics and conflict topics were selected.
2. fNIRS data collection
    1. Use 26-channel fNIRS topography system (see **Table of Materials**) to collect fNIRS data.
        NOTE: Two customized optode probes set covered the bilateral frontal, temporal, and parietal cortices (**Figure 1B**).
    2. Precisely, ask each participant to wear a cap with two customized probe sets (see **Table of Materials**).
    3. Align the nasion, inion, and ear mastoids with Fpz, Opz, T7, and T8, which are typical landmarks of 10-20 international system[26].
    4. Align channel (CH) 11 to T3 and CH25 to T4 following the international 10-20 system for the two probe sets[27,28].
    5. Validate the anatomical locations of probe sets by scanning magnetic resonance imaging (MRI) data from a typical participant with a high-resolution T1-weighted magnetization-prepared rapid gradient-echo sequence (TR = 2530 ms; TE = 3.39 ms; flip

angle = 7°; slice thickness = 1.3 mm; voxel size = 1.3 x 1 x 1.3 mm).

6. Use Statistical Parametric Mapping 12 (SPM12) to normalize the image to standard Montreal imaging institute coordinate (MNI coordinate) space[29]. Then, use the NIRS_SPM toolbox (see **Table of Materials**) to project the MNI coordinates of the probes to the automated anatomical labeling (AAL) template.

7. Collect the optical density data of near-infrared light at three wavelengths (780, 805, and 830 nm) at a sampling rate of 55.6 Hz (equipment default parameters).

8. Test the signal quality by using fNIRS topography system built-in equipment software (see **Table of Materials**).

9. Begin signal recording.
   NOTE: Some published protocols have demonstrated how to collect fNIRS signals with various equipment and systems[30,31,32].

3. fNIRS data preprocessing

   1. Export the data files from the equipment.
      NOTE: In the current experiment, the built-in software automatically converted all-optical density data into oxyhemoglobin (HbO) concentration changes based on the modified Beer-Lambert law.

   2. Remove the first and last 15 s of data for each session to avoid transient responses.

   3. Use the MATLAB decimate built-in function to downsample the data from 55.6 Hz to 11.1 Hz.
      NOTE: The power spectrum patterns between 55.6 Hz and 11.1 Hz are quite similar (**Supplementary Figure 1**).

   4. Use the built-in MATLAB application function (Homer3, see **Table of Materials**) with appropriate filtering function to apply the discrete wavelet transform filter method to correct motion artifacts.

   5. Use the MATLAB pca built-in function to remove global physiological noise. Remove the top 80% of the variance from the signals.

   6. Remove physiological noise based on the previous studies[33]. Precisely, remove frequency bands of each signal above 0.7 Hz to avoid aliasing of high-frequency physiological noise (e.g., cardiac activity).

   7. Then, remove frequency bands of each signal below 0.01 Hz to filter out very-low-frequency fluctuations.

   8. Finally, remove frequency bands of each signal within 0.15-0.3 Hz to exclude the potential impact of respiratory activity.

4. First-level fNIRS Data Processing

   1. First, calculate INS using traditional WTC (INS_{WTC}).
      NOTE: Here, a women-led time-lagged pattern of INS_{WTC} was predicted to occur between the brain activity of women and that of men because previous studies have suggested different roles of women and men during a conversation[34,35]. The traditional WTC calculated this pattern of INS_{WTC} by shifting the brain activity of men backward relative to that of women (see **Equation 2**).

   2. Calculate the women-led 2 s-lagged INS_{WTC} value after removing the initial 2 s of data from women

and the last 2 s of data from men with **Equation 2**. Similarly, after removing the initial 2 s of data from men and the last 2 s of data from women, calculate the men-led 2 s-lagged INS_{WTC} value with **Equation 4**.

NOTE: Here, the wcoherence function, which is a built-in function of the wavelet toolbox of MATLAB, was used (see **Table of Materials**).

3. Repeat this procedure with different time lags n, i.e., n = 2 s, 4 s, 6 s, 8 s across all potential CH pairs (e.g., CH2 in women and CH10 in men, 676 pairs in total). Additionally, calculate the strength of men-led time-lagged INS_{WTC} the same way (**Equation 4**).

$$WTC(M_t, W_{t+n}) = \frac{|S(C^*_{M_t}(i,t) \cdot C_{W_{t+n}}(i,t))|^2}{S(|C_{M_t}(i,t)|^2) \cdot S(|C_{W_{t+n}}(i,t)|^2)}$$

4. Second, calculate INS using pWTC (INS_{pWTC}).

NOTE: pWTC was calculated based on **Equation 3**. The calculation of INS_{pWTC} was repeated with different time lags n, i.e., n = 2 s, 4 s, 6 s, 8 s across all potential channel pairs (e.g., CH2 in women and CH10 in men, 676 pairs in total). Additionally, the strength of the men-led time-lagged INS_{pWTC} was calculated the same way (**Equation 5**).

$$pWTC_{MtoW} = \frac{\left|\sqrt{WTC(M_t, W_{t+n})} - \sqrt{WTC(W_t, W_{t+n})} \cdot \sqrt{WTC(M_t, W_t)}^*\right|^2}{[1 - WTC(W_t, W_{t+n})] \cdot [1 - WTC(M_t, W_t)]}$$

5. Generate time-lagged time series of fNIRS signals at different time lags.

6. Calculate the values of the time-lagged WTC at different time lags.

7. Generate autocorrelated time series of fNIRS signals at different time lags. To calculate the 2 s-autocorrelated value for men, remove the first 2 s of data from the men and the last 2 s data from the men.

8. Calculate the autocorrelated WTC values at different time lags.

9. Generate time-aligned time series of fNIRS signals at different time lags. To calculate the 2 s time-aligned WTC, remove the first 2 s of data from the men and the women's first 2 s of data.

10. Calculate the time-aligned WTC values.

11. Enter time-aligned WTC, time-lagged WTC, and autocorrelated WTC values at different time lag into **Equation 3** and **Equation 5**-the equation of pWTC, generating INS_{pWTC}.

12. Finally, calculate INS using the GC method (INS_{GC}).

NOTE: To further validate the pWTC method and evaluate its advantages and disadvantages, GC-based INS was calculated using the GC method (INS_{GC}).

13. Based on the pWTC result, bandpass filters the HbO signal of each individual at the SMC (i.e., 0.4-0.6 Hz, see **Representative Results**).

14. Conduct a GC test (Econometric toolbox, MATLAB) within each dyad in the supportive and conflict topics separately.

NOTE: Four groups of F-values are obtained for INS_{GC}: (1) from women to men on the supportive topic (W2M_supp); (2) from men to women on the supportive topic (M2W_supp); (3) from women to men on the conflict topic (W2M_conf); and (4) from men to women on the conflict topic (M2 W_conf). The F-values are used to index the INS_{GC}.

5. Second-level fNIRS data processing

    1. Transform INS with Fisher-z transformation, and then average INS at the temporal dimension.

        NOTE: Here, Fisher-z transformation was conducted using a custom MATLAB script with **Equation 6**[36]:

        $$z = \frac{1}{2} \cdot \ln\left(\frac{1+r}{1-r}\right)$$

        where, r is the value of the WTC or pWTC, and z is the Fisher-z transformed value of the WTC or pWTC.

    2. For the averaged INS at each time lag, conduct a paired two-sample *t*-test (supportive *vs*. conflict) on each CH pair across the frequency range. Then, identify all significant frequency clusters ($P < 0.05$).

    3. Conduct a cluster-based permutation test to establish a threshold for the results.

        1. Reassign dyadic relationships by randomly assigning the participants to new two-member pairs, i.e., the participants of a dyad that had never communicated with one another. Recalculate the INS at each time lag, perform paired *t*-tests again in the new sample, and identify significant frequency clusters again.

        2. Select the cluster with the largest summed t-value. Repeat the above procedures 1000 times to generate a null distribution of the maximum false-positive t-values.

            NOTE: The distribution is served as the chance level. The familywise error rate (FWER) is controlled at $q = 0.05$, which means that only the top 5% of the null distribution of the false-positive t-values exceeds the threshold (R*).

        3. Compare the summed t-value of each identified frequency cluster in the original sample with the null distribution to obtain significant statistical results.

    4. Conduct a context (supportive, conflict) x direction (women to men, men to women) analysis of variance (ANOVA) to test the difference in INS direction between different conditions (i.e., topics) ($p < 0.05$).

    5. Conduct a paired two-sample two-tailed t-test between the results of WTC (Wt, Mt + n) and WTC (Mt, Mt + n) to test the potential impact of autocorrelation on INS.

        NOTE: The INS of WTC (Mt, Mt + n) reflects autocorrelation.

Representative Results

Simulation results

The results showed that the time-lagged INS_{WTC} with autocorrelation was significantly higher than the time-lagged INS_{WTC} without autocorrelation ($t(1998) = 4.696$, $p < 0.001$) and time-lagged INS_{pWTC} ($t(1998) = 5.098$, $p < 0.001$). Additionally, there was no significant difference between time-lagged INS_{WTC} without autocorrelation and INS_{pWTC} ($t(1998) = 1.573$, $p = 0.114$, **Figure 2A**). These results indicate that pWTC can effectively remove the impact of the autocorrelation effect on INS. Additionally, when the WTC value was set to be close to 0 or 1, the time-lagged INS_{pWTC} still showed reliable results when the WTC value was away from 0 or 1 (**Supplementary Figure 2).**

Empirical experiment results

INS pattern using the traditional WTC method

The results showed that at 0.04-0.09 Hz,INS_{WTC}in the sensorimotor cortex (SMC, CH20) of both women and men

was significantly higher in the supportive topic than in the conflict topic when the brain activity of men lagged behind that of women by 2 s, 4 s, and 6 s (2 s: $t(21) = 3.551$, $p = 0.0019$; lag 4 s: $t(21) = 3.837$, $p = 0.0009$; lag 6 s: $t(21) = 3.725$, $p = 0.0013$). Additionally, at 0.4-0.6 Hz, INS_{WTC} in the SMC was significantly higher in the conflict topic than in the supportive topic when men's brain activity lagged behind women's by 4 s ($t(21) = 2.828$, $p = 0.01$, **Figure 2B**).

Additionally, to compare the direction of INS_{WTC} in different topics, a topic (supportive, conflict) x direction (women to men, men to women) ANOVA was first conducted on INS_{WTC} of the SMC under a 2-6 s time lag. The 0.04-0.09 Hz results did not show any significant interaction effects at any time lag (*ps* > 0.05). For the 0.4-0.6 Hz frequency range, the results showed that the interaction effect was marginally significant ($F(1, 21) = 3.23$, $p = 0.086$). Pairwise comparisons showed that INS_{WTC} from women to men was significantly higher in the conflict topic than in the supportive topic (*M.D.* = 0.014, *S.E.* = 0.005, $p = 0.015$), whereas INS_{WTC} from men to women did not differ significantly between topics (*M.D.* = 0.002, *S.E.* = 0.006, $p = 0.695$).

Finally, to test the impact of autocorrelation on the results of traditional time-lagged INS_{WTC}, INS_{WTC} was compared between $WTC(W_t, M_{t+4})$ and $WTC(M_t, M_{t+4})$ at 0.04-0.09 Hz and 0.4-0.6 Hz, respectively. Note that the INS_{WTC} of $WTC(M_t, M_{t+4})$ reflects autocorrelation. The results showed that at the 0.4-0.6 Hz, there was no significant difference between the INS_{WTC} of $WTC(W_t, M_{t+4})$ and that of $WTC(M_t, M_{t+4})$ ($t(21) = 0.336$, $p = 0.740$). At 0.04-0.09 Hz, the INS_{WTC} of *WTC(Mt, Mt+4)* was significantly higher than that of $WTC(W_t, M_{t+4})$ ($t(21) = 4.064$, $p < 0.001$). A comparison was also conducted between the frequency ranges of 0.04-0.09 Hz and 0.4-0.6 Hz regarding INS_{WTC} of $WTC(M_t, M_{t+4})$. The results showed that the INS_{WTC} of $WTC(M_t, M_{t+4})$ was significantly higher at 0.04-0.09 Hz than at the 0.4-0.6 Hz ($t(21) = 5.421$, $p < 0.001$). These results indicate that the time-lagged INS_{WTC} was affected by autocorrelation in both the low- and high-frequency ranges, but the impact was larger for the lower-frequency range than for the higher-frequency range.

INS pattern using the pWTC method

The results showed that the difference in INS_{pWTC} between the conflict and supportive topics reached significance at the SMC of both women and men at 0.4-0.6 Hz when male brain activity lagged behind that of women by 4 s ($t(21) = 4.224$, $p = 0.0003$). At 0.04-0.09 Hz; however, no significant results were found, nor were their effective results at other frequency ranges (*Ps* > 0.05, **Figure 2C**).

An additional ANOVA test was conducted on the INS_{pWTC} of the SMC at 0.4-0.6 Hz. The results showed that the interaction between topic and direction was marginally significant ($F(1,21) = 3.48$, $p = 0.076$). Further pairwise comparisons showed that INS_{pWTC} from women to men was significantly higher in the conflict topic than in the supportive topic (*M.D.* = 0.016, *S.E.* = 0.004, $p = 0.002$), whereas INS_{pWTC} from men to women did not differ significantly between topics (*M.D.* = 0.0007, *S.E.* = 0.006, $p = 0.907$, **Figure 2D**).

INS pattern using the GC method

An ANOVA test was conducted on the INS_{GC} at the SMC within the 0.4-0.6 Hz only. The results showed a significant interaction between topic and direction ($F(1,21) = 8.116$, $p = 0.010$). Pairwise analysis showed that INS_{GC} from women to men was significantly higher in the conflict topic than in the supportive topic ($MD = 5.50$, $SE = 2.61$, $p = 0.043$). In contrast,

the INS_{GC} from men to women was not significantly different between topics (*MD* = 1.42, *SE* = 2.61, *p* = 0.591, **Figure 2E**).

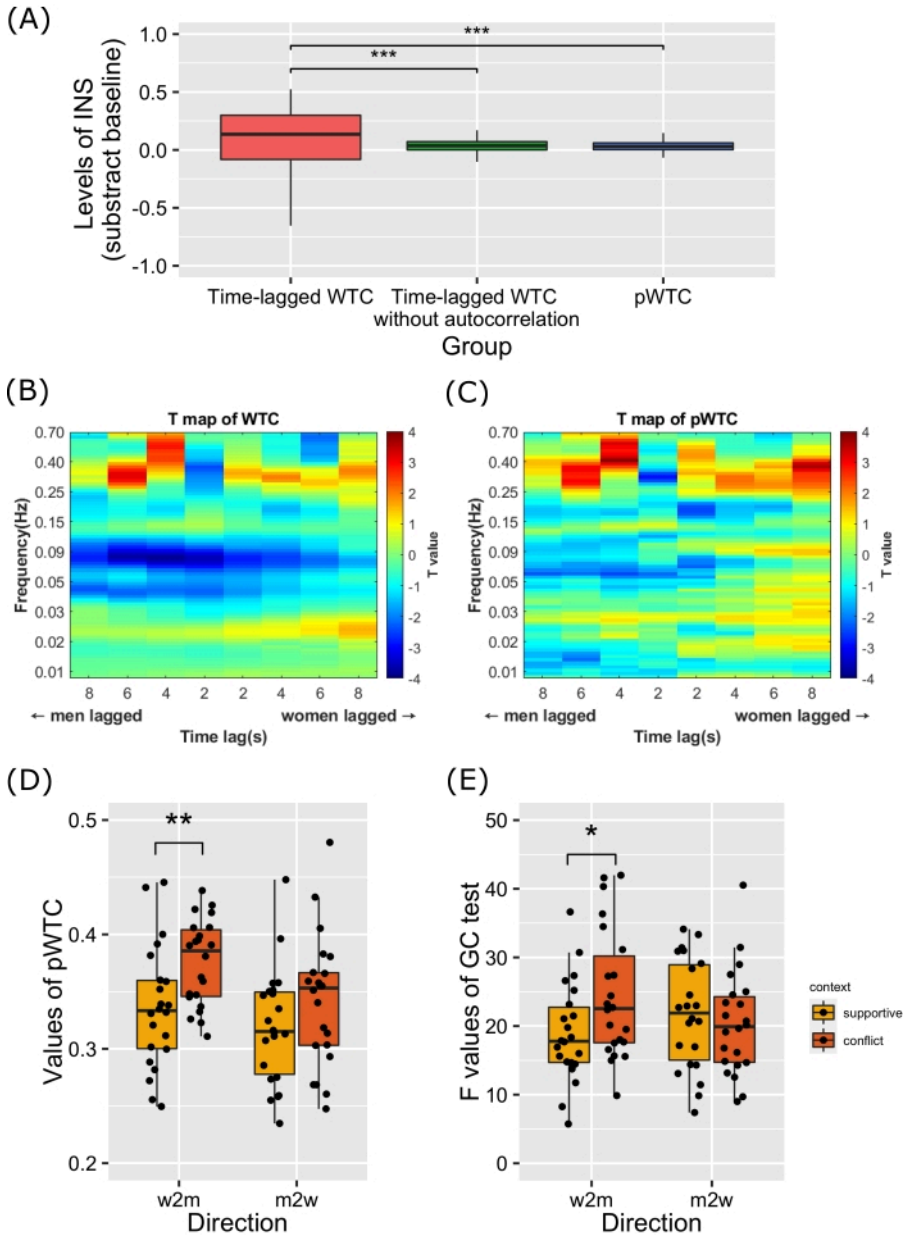

Figure 2: Results of the simulation and empirical experiment. (**A**) The simulation results of three simulated samples. The time-lagged INS_{WTC} with autocorrelation was significantly higher than time-lagged INS_{WTC} without autocorrelation and INS_{pWTC}. There was no significant difference between time-lagged INS_{WTC} without autocorrelation and pWTC. (**B**) The t-map of INS_{WTC} in the empirical experiment, showing significant context effects within 0.04-0.09 Hz when SMC activity of men lagged behind that of women by 2-6 s. There was also a marginally considerable context effect within 0.4-0.6 Hz when

SMC activity of men lagged behind that of women by 4 s. (**C**) The t-map of INS_{pWTC}, showing a significant context effect within 0.4-0.6 Hz when SMC activity of men lagged behind that of women by 4 s. (**D**) Comparison of directional INS_{pWTC} at different topics by pWTC. Directional INS from women to men is significantly higher in conflict contexts than in supportive contexts. (**E**) Validation of directional INS by GC test (INS_{GC}). The resulting pattern of INS_{GC} is similar to INS_{pWTC}. Please click here to view a larger version of this figure.

Supplementary Figure 1: The power spectrum plot for sample rate at 11.1 Hz (blue line) and 55.6 Hz (red line). The power spectrum pattern for the two is quite similar. Please click here to download this File.

Supplementary Figure 2: The pWTC maps of floor and ceil WTC. (**A**) Left panel: the time-lagged WTC map generated by two same signals, the x-axis is time point, and the y-axis is frequency-band. The mean value of WTC at all points is ~1. Right panel: the pWTC map of two similar signals. The pWTC map is quite similar to the WTC map. (**B**) Left panel: the time-lagged WTC map generated by two random signals, the x-axis is the time point, and the y-axis is the frequency-band. The mean value of WTC at all points is ~0. Right panel: the pWTC map of two similar signals. The pWTC map is quite similar to the WTC map. Please click here to download this File.

Discussion

In hyperscanning studies, it is usually essential to describe the directional and temporal patterns of information flow between individuals. Most previous fNIRS hyperscanning studies have used traditional WTC[25] to infer these characteristics by calculating the time-lagged INS. However, as one of the intrinsic features of the fNIRS signal[20,21], the autocorrelation effect might confound the time-lagged INS. To address this issue, in the protocol herein, a method termed pWTC was introduced[22]. This method estimates the time-lagged INS after partially out autocorrelation and maintains the advantages of the WTC method. This protocol offers step-by-step guidance on how to conduct pWTC and validates the results of pWTC by comparing its results with those of traditional WTC and GC tests.

The critical steps of applying pWTC in fNIRS-based hyperscanning data are demonstrated in this protocol. Specifically, first, to calculate the time-lagged WTC, the autocorrelated WTC, and time-aligned WTC must be calculated based on the time-lagged fNIRS time series. Next, the pWTC are computed at different time lags according to **Equation 1**. The results of the pWTC return a time x frequency matrix, and the values in the matrix ranges from 0 to 1. Thus, further statistical tests can be conducted on these values.

In the demonstration protocol, the representative results of the traditional WTC showed two significant effects at two frequency bands: 0.4-0.6 Hz. However, the impact within the 0.04-0.09 Hz did not survive the threshold in the pWTC results, suggesting that this effect might be confounded by the autocorrelation effect of the fNIRS signal. On the other hand, the results within the 0.4-0.6 Hz range were well replicated by the pWTC method. These results indicate that after removing the autocorrelation effect, pWTC provides more sensitive and specific developments in inferring INS's directional and temporal patterns between individuals. Another possibility, however, is that pWTC is not susceptible to INS's directional and temporal patterns in lower frequency ranges than in the higher frequency ranges, resulting in underestimation of

the INS effect. Future studies are needed to clarify these possibilities further.

A comparison with the GC test further supports this conclusion. The results of the GC test were quite similar to those of the pWTC, showing important information flow from women to men but not from men to women. There was a slight difference between the results of the GC test and pWTC, i.e., the interaction effect between topic and direction was marginally significant in the results of the pWTC but reached significance in the GC test. This difference may be because the pWTC is calculated at a finer timescale than the GC test. Thus, although both the pWTC and GC tests can provide reliable results when controlling for the autocorrelation effect, the pWTC is advantageous because it is not necessary to make stationary assumptions and holds a high temporal-spectrum structure.

The pWTC method also has its limitations. Similar to the GC test, the causality inferred from pWTC is not a real causality[37,38]. Instead, it only indicates a temporal relationship between the signals of A and B. This issue should be kept in mind when applying the pWTC method. Second, pWTC only partials out the autocorrelation effect. Thus, other potential concurrent variables, such as shared environments or similar actions, may still impact the results. Consequently, conclusions about the direction and temporal pattern of information flow should be drawn after controlling these confounding factors.

Additionally, there were some complicated issues about fNIRS data preprocessing. Although fNIRS has a high tolerance of head movements, motion artifacts are still the most significant source of the noise[39]. Large head movements would still lead to a position shift of the optodes, generating motion artifacts such as sharp spike and baseline shifts. To address these issues, many artifacts correction approaches were developed such as spline interpolation[40], wavelet-based filtering[39], principle component analysis[41], and correlation-based signal improvement[42], etc. Cooper and his collegues[43] have compared these approaches based on real resting-state fNIRS data and found that wavelet-based filtering produced the highest increase in contrast-to-noise ratio. Further, Brigadoi and her collegues[44] have also compared these approaches in real linguistic task data and also found that wavelet-based filtering was the most effective approach in correcting motion artifacts. Thus, in this study, wavelet-based filtering was applied and also recommended for future fNIRS hyperscanning studies.

In general, pWTC is a valuable approach in estimating the directional and temporal patterns of information flow during social interaction. More importantly, it is believed that the pWTC method is also suitable for pseudo-hyperscanning studies (i.e., signals of two or multiple brains are not collected simultaneously[45,46]). In such experiments, although the direction of information flow is fixed, it is also of interest to examine the duration of the time lag between the input of the signal and the process of the signal. Therefore, autocorrelation can also confound the results of the time-lagged INS. In the future, this method can answer many questions in hyperscanning and other interbrain studies. For example, to determine the dominant role in various social relationships, such as teachers and students, doctors and patients, and performers and audiences. Additionally, as pWTC maintains the temporal structures of INS, it is also possible to test the dynamic pattern of INS, such as group attitude convergence.

Disclosures

The authors declare no competing financial interests.

Acknowledgments

This work was supported by the National Natural Science Foundation of China (61977008) and the Young Top Notch Talents of Ten Thousand Talent Program.

References

1. Hasson, U., Ghazanfar, A. A., Galantucci, B., Garrod, S., Keysers, C. Brain-to-brain coupling: A mechanism for creating and sharing a social world. *Trends in Cognitive Sciences.* **16** (2), 114-121 (2012).
2. Hasson, U., Frith, C. D. Mirroring and beyond: Coupled dynamics as a generalized framework for modelling social interactions. *Philosophical Transactions of the Royal Society B: Biological Sciences.* **371**, 20150366 (2016).
3. Jiang, J. et al. Neural synchronization during face-to-face communication. *Journal of Neuroscience.* **32** (45), 16064-16069 (2012).
4. Jiang, J. et al. Leader emergence through interpersonal neural synchronization. *Proceedings of the National Academy of Sciences of the United States of America.* **112** (14), 4274-4279 (2015).
5. Dai, B. et al. Neural mechanisms for selectively tuning in to the target speaker in a naturalistic noisy situation. *Nature Communications.* **9** (1), 1-12 (2018).
6. Long, Y. et al. Interpersonal neural synchronization during interpersonal touch underlies affiliative pair bonding between romantic couples. *Cerebral Cortex (New York, N.Y. : 1991).* **31** (3), 1647-1659 (2021).
7. Liu, W. et al. Shared neural representations of syntax during online dyadic communication. *NeuroImage.* **198**, 63-72 (2019).
8. Zheng, L. et al. Enhancement of teaching outcome through neural prediction of the students' knowledge state. *Human Brain Mapping.* **39** (7), 3046-3057 (2018).
9. Stephens, G. J., Silbert, L. J., Hasson, U. Speaker-listener neural coupling underlies successful communication. *Proceedings of the National Academy of Sciences of the United States of America.* **107** (32), 14425-14430 (2010).
10. Hirsch, J. et al. Interpersonal agreement and disagreement during face-to-face dialogue: An fNIRS investigation. *Frontiers in Human Neuroscience.* **14**, 606397 (2021).
11. Pan, Y., Cheng, X., Zhang, Z., Li, X., Hu, Y. Cooperation in lovers: An fNIRS-based hyperscanning study. *Human Brain Mapping.* **38** (2), 831-841 (2017).
12. Cui, X., Bryant, D. M., Reiss, A. L. NIRS-based hyperscanning reveals increased interpersonal coherence in superior frontal cortex during cooperation. *NeuroImage.* **59** (3), 2430-2437 (2012).
13. Piazza, E. A., Hasenfratz, L., Hasson, U., Lew-Williams, C. Infant and Adult Brains Are Coupled to the Dynamics of Natural Communication. *Psychological Science.* **31** (1), 6-17 (2020).
14. Djalovski, A., Dumas, G., Kinreich, S., Feldman, R. Human attachments shape interbrain synchrony toward efficient performance of social goals. *NeuroImage.* **226**, 117600 (2021).

15. Zhao, H. et al. How mother-child interactions are associated with a child's compliance. *Cerebral Cortex.* **31** (9), 4398-4410 (2021).

16. Jiang, J., Zheng, L., Lu, C. A hierarchical model for interpersonal verbal communication. *Social Cognitive and Affective Neuroscience.* **16** (1-2), 246-255 (2021).

17. Yan, W. et al. Bibliometric evaluation of 2000-2019 publications on functional near-infrared spectroscopy. *NeuroImage.* **220**, 117121 (2020).

18. Zheng, L. et al. Affiliative bonding between teachers and students through interpersonal synchronisation in brain activity. *Social Cognitive and Affective Neuroscience.* **15** (1), 97-109 (2020).

19. Dean, R. T., Dunsmuir, W. T. M. Dangers and uses of cross-correlation in analyzing time series in perception, performance, movement, and neuroscience: The importance of constructing transfer function autoregressive models. *Behavior Research Methods.* **48** (2), 783-802 (2016).

20. Barker, J. W., Rosso, A. L., Sparto, P. J., Huppert, T. J. Correction of motion artifacts and serial correlations for real-time functional near-infrared spectroscopy. *Neurophotonics.* **3** (3), 031410 (2016).

21. Huppert, T. J. Commentary on the statistical properties of noise and its implication on general linear models in functional near-infrared spectroscopy. *Neurophotonics.* **3** (1), 010401 (2016).

22. Mihanović, H., Orlić, M., Pasarić, Z. Diurnal thermocline oscillations driven by tidal flow around an island in the Middle Adriatic. *Journal of Marine Systems.* **78** (SUPPL. 1), S157-S168 (2009).

23. Ng, E. K. W., Chan, J. C. L. Geophysical applications of partial wavelet coherence and multiple wavelet coherence. *Journal of Atmospheric and Oceanic Technology.* **29** (12), 1845-1853 (2012).

24. Ng, E. K. W., Chan, J. C. L. Interannual variations of tropical cyclone activity over the north Indian Ocean. *International Journal of Climatology.* **32** (6), 819-830 (2012).

25. Grinsted, A., Moore, J. C., Jevrejeva, S. Application of the cross wavelet transform and wavelet coherence to geophysical time series. *Nonlinear Processes in Geophysics.* **11** (5/6), 561-566 (2004).

26. Jurcak, V., Tsuzuki, D., Dan, I. 10/20, 10/10, and 10/5 systems revisited: Their validity as relative head-surface-based positioning systems. *NeuroImage.* **34** (4), 1600-1611 (2007).

27. Homan, R. W., Herman, J., Purdy, P. Cerebral location of international 10-20 system electrode placement. *Electroencephalography and Clinical Neurophysiology.* **66** (4), 376-382 (1987).

28. Koessler, L. et al. Automated cortical projection of EEG sensors: Anatomical correlation via the international 10-10 system. *NeuroImage.* **46** (1), 64-72 (2009).

29. Penny, W., Friston, K., Ashburner, J., Kiebel, S., Nichols, T. *Statistical Parametric Mapping: The Analysis of Functional Brain Images.* Academic Press (2007).

30. Shalinsky, M. H., Kovelman, I., Berens, M. S., Petitto, L. A. Exploring cognitive functions in babies, children & adults with near infrared spectroscopy. *Journal of Visualized Experiments: JoVE.* **29**, e1268 (2009).

31. Xu, S. Y., Cheong, L. I., Zhuang, Y., Couto, T. A. P., Yuan, Z. Conducting concurrent electroencephalography

and functional near-infrared spectroscopy recordings with a flanker task. *Journal of Visualized Experiments: JoVE.* **159**, e60669 (2020).

32. Noah, J. A. et al. fMRI validation of fNIRS measurements during a naturalistic task. *Journal of Visualized Experiments: JoVE.* **100**, e52116 (2015).
33. Tong, Y., Lindsey, K. P., Frederick, B. D. Partitioning of physiological noise signals in the brain with concurrent near-infrared spectroscopy and fMRI. *Journal of Cerebral Blood Flow and Metabolism.* **31** (12), 2352-2362 (2011).
34. Buck, R., Miller, R. E., Caul, W. F. Sex, personality, and physiological variables in the communication of affect via facial expression. *Journal of Personality and Social Psychology.* **30** (4), 587-596 (1974).
35. Walen, H. R., Lachman, M. E. Social support and strain from partner, family, and friends: Costs and benefits for men and women in adulthood. *Journal of Social and Personal Relationships.* **17** (1), 5-30 (2000).
36. Chang, C., Glover, G. H. Time-frequency dynamics of resting-state brain connectivity measured with fMRI. *NeuroImage.* **50** (1), 81-98 (2010).
37. Liu, H. et al. Inferring subsurface preferential flow features from a wavelet analysis of hydrological signals in the shale hills catchment. *Water Resources Research.* **56** (11), 0-3 (2020).
38. Rhif, M., Abbes, A. B., Farah, I. R., Martínez, B., Sang, Y. Wavelet transform application for/in non-stationary time-series analysis: A review. *Applied Sciences (Switzerland).* **9** (7), 1345 (2019).
39. Molavi, B., Dumont, G. A. Wavelet-based motion artifact removal for functional near-infrared spectroscopy. *Physiological Measurement.* **33** (2), 259-270 (2012).
40. Scholkmann, F., Spichtig, S., Muehlemann, T., Wolf, M. How to detect and reduce movement artifacts in near-infrared imaging using moving standard deviation and spline interpolation. *Physiological Measurement.* **31** (5), 649-662 (2010).
41. Zhang, Y., Brooks, D. H., Franceschini, M. A., Boas, D. A. Eigenvector-based spatial filtering for reduction of physiological interference in diffuse optical imaging. *Journal of Biomedical Optics.* **10** (1), 011014 (2005).
42. Cui, X., Bray, S., Reiss, A. L. Functional near infrared spectroscopy (NIRS) signal improvement based on negative correlation between oxygenated and deoxygenated hemoglobin dynamics. *NeuroImage.* **49** (4), 3039-3046 (2010).
43. Cooper, R. J. et al. A systematic comparison of motion artifact correction techniques for functional near-infrared spectroscopy. *Frontiers in Neuroscience.* **0** (OCT), 147 (2012).
44. Brigadoi, S. et al. Motion artifacts in functional near-infrared spectroscopy: A comparison of motion correction techniques applied to real cognitive data. *NeuroImage.* **85**, 181-191 (2014).
45. Liu, Y. et al. Measuring speaker-listener neural coupling with functional near infrared spectroscopy. *Scientific Reports.* **7** (October 2016), 1-13 (2017).
46. Li, Z. et al. Speaker-listener neural coupling reveals an adaptive mechanism for speech comprehension in a noisy environment. *Cerebral Cortex.* bhab118 (2021).